Statistical approach of weakly nonlinear ablative Rayleigh–Taylor instability

J. Garnier[a)]
Laboratoire de Probabilités et Modèles Aléatoires & Laboratoire Jacques-Louis Lions, Université Paris VII, 2 Place Jussieu, 75251 Paris Cedex 05, France

L. Masse
Commissariat à l'Energie Atomique, Direction des Applications Militaires, Boîte Postale 12, 91680 Bruyères le Châtel, France

(Received 4 January 2005; accepted 14 April 2005; published online 8 June 2005)

A weakly nonlinear model is proposed for the Rayleigh–Taylor instability in presence of ablation and thermal transport. The nonlinear effects for a single-mode disturbance are computed, included the nonlinear correction to the exponential growth of the fundamental modulation. Mode coupling in the spectrum of a multimode disturbance is thoroughly analyzed by a statistical approach. The exponential growth of the linear regime is shown to be reduced by the nonlinear mode coupling. The saturation amplitude is around 0.1λ for long wavelengths, but higher for short instable wavelengths in the ablative regime. © *2005 American Institute of Physics*. [DOI: 10.1063/1.1927542]

I. INTRODUCTION

The Rayleigh–Taylor (RT) instability occurs when a fluid accelerates another fluid of higher density. This phenomenon may dramatically reduce the performance of inertial confinement fusion (ICF) experiments by degrading the symmetry of implosion.[1] In ICF ablation plays a central role.[2] It has been shown by several authors that the ablative RT instability growth is stabilized relative to classical RT during the linear stage, where the growth is exponential in time. The self-consistent theory has shown a complicated dependence of the growth rate on the plasma parameters.[3,4] In this paper a weakly nonlinear (WNL) theory is developed for the ablative RT instability. The first WNL analysis in a simplified framework was performed in Ref. 5. We aim at deriving closed-form expressions for the most important physical quantities. The simplest and most studied case is that of a single-mode perturbation. A third-order WNL analysis of the single-mode case was presented in Ref. 6 in the limit of a very large density ratio. We derive in Sec. III analytic formulas for the second and third harmonic generation efficiency and the nonlinear correction to the exponential growth of the fundamental modulation for arbitrary Atwood numbers. A suitable choice of the self-consistent Atwood number then gives accurate results relevant to ICF. In the multimode case we also give in Sec. IV the expression of the interface elevation taking into account the mode coupling. Recently a WNL theory was presented in the framework of a finite bandwidth[7] where the results can only be integrated numerically. We show that it is necessary to compute the third-order WNL corrections in the multimode case to capture the first statistical corrections. We get expressions for the saturation amplitudes which show that short-wavelength modes saturate at a significantly higher amplitude (compared to the wavelength) than long-wavelength modes. We finally report in Sec. V the results of simulations performed with a two-dimensional (2D) Lagrangian code which confirm the theoretical predictions.

II. WEAKLY NONLINEAR ANALYSIS

In the standard case where the ablative flow is subsonic we can apply the isobaric approximation[8] so that the fluid dynamics is governed by the system of conservation laws for mass, x and $\mathbf{y}$ momenta, and energy,

$$\partial_t\rho + \partial_x(\rho u) + \nabla_y.(\rho\mathbf{v}) = 0, \tag{1}$$

$$\partial_t(\rho u) + \partial_x(\rho u^2 + p) + \nabla_y.(\rho u\mathbf{v}) = \rho g, \tag{2}$$

$$\partial_t(\rho\mathbf{v}) + \partial_x(\rho u\mathbf{v}) + \nabla_y.(\rho\mathbf{v}\otimes\mathbf{v} + p) = 0, \tag{3}$$

$$C_p[\partial_t(\rho T) + \partial_x(\rho u T) + \nabla_y.(\rho\mathbf{v}T)] = \partial_x q_x + \nabla_y.q_\mathbf{y}, \tag{4}$$

where ρ is the density, u (resp. $\mathbf{v}$) is the fluid velocity in the x (resp. y) direction, p is the pressure, T is the temperature, $q_x = \lambda\partial_x T$ and $q_y = \lambda\nabla_y T$ are the heat flows in the x (resp. y) direction, C_p is the specific heat per unit mass at constant pressure, and λ is the thermal conductivity. Gravity g points into the x direction.

Our model belongs to the family of the sharp boundary models (SBM).[8–10] The forthcoming analysis is based on a set of three hypotheses. First we assume that the unperturbed flow is stationary and one dimensional. The ablation front is represented as a zero-thickness surface for the hydrodynamic variables $(\rho, u, \mathbf{v}, p)$ which separates a cool material with high density ρ_L on the left side and a blowoff plasma with low density ρ_R on the right side. In the point of view of the temperature the ablation front is an isotherm. The SBM approximation is applied to the hydrodynamic variables and not to the temperature. As a result the temperature and heat flow are continuous. Second, we assume that the density ρ and the thermal conductivity λ are constant on both sides of the ablation front (see Fig. 1). Finally we assume that the thermal transport is small in the overdense region, and that it is large in the blowoff region. This hypothesis reads as

[a)]Electronic mail: garnier@math.jussieu.fr

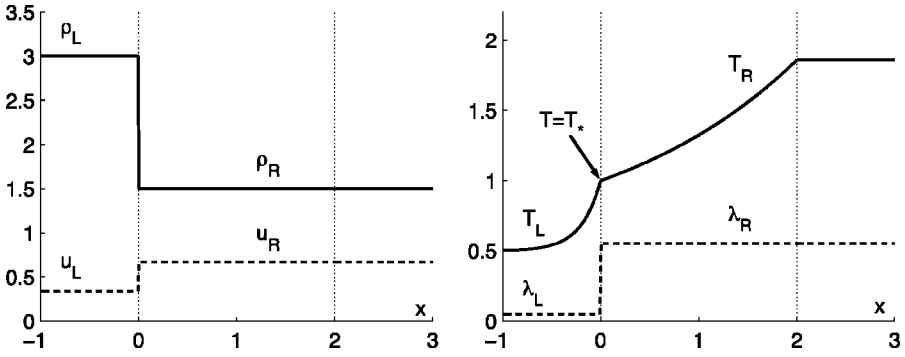

FIG. 1. Unperturbed one-dimensional stationary flow in dimensionless units. $x=0$ (resp. $x=2$) is the position of the ablation front (resp. absorption front).

$d_L|\mathbf{k}| \ll 1 \ll d_R|\mathbf{k}|$, where $\mathbf{k}$ is the typical wave number of the interface modulation, $d_{L,R}=\lambda_{L,R}/(\dot{m}C_p)$ are the left and right thermal diffusion lengths, and $\dot{m}$ is the mass ablation rate. This model has been shown to reproduce accurately the linear growths of RT instabilities obtained by the self-consistent linear theory[3,4] if the jump density is calculated in a self-consistent way.[11,12] We show in this paper that a WNL analysis of this model can be performed at any order without any more assumption.

We study the growth of a small-amplitude perturbation of the interface whose displacement with respect to the unperturbed front $x=0$ is described by $x=\eta(t,\mathbf{y})$. The typical amplitude δ of the initial disturbance is assumed to be small (i.e., smaller than its typical wavelength). The interface displacement η, the hydrodynamic variables $U=(u,\mathbf{v},p)$, and the temperature T can be expanded in powers of δ as

$$\eta(t,\mathbf{y}) = \delta\eta_1(t,\mathbf{y}) + \delta^2\eta_2(t,\mathbf{y}) + \delta^3\eta_3(t,\mathbf{y}) + O(\delta^4),$$

$$U(t,x,\mathbf{y}) = U_0(x) + \delta U_1(t,x,\mathbf{y}) + \delta^2 U_2(t,x,\mathbf{y}) + \delta^3 U_3(t,x,\mathbf{y}) + O(\delta^4).$$

Substituting these ansätze into the system (1)–(4) and collecting the terms with the same powers in δ, we get for terms of order δ the system governing the linear stability of the unperturbed solution $(U_0,T_0,\eta_0=0)$. The terms of order δ^2 (resp. δ^3) give the second-order (resp. third-order) WNL corrections. The governing equations and the jump conditions satisfied by the hydrodynamic variables U_j are derived from Eqs. (1)–(3) in the . Equation (4) then determines the temperature profiles T_j in the two regions. The interface is defined as the isotherm $T=\overline{T_*}$, so the continuity of the temperature imposes

$$T_R[t,x=\eta(t,\mathbf{y})^+,\mathbf{y}] = T_L[t,x=\eta(t,\mathbf{y})^-,\mathbf{y}] = \overline{T_*}. \tag{5}$$

Besides the continuity of the heat flow reads at the interface $[\lambda\mathbf{n}\cdot\boldsymbol{\nabla}T]_\eta=0$ where $[\phi]_\eta=\phi[t,x=\eta(t,\mathbf{y})^+,\mathbf{y}]-\phi[t,x=\eta(t,\mathbf{y})^-,\mathbf{y}]$ and $\mathbf{n}$ is the unit normal vector,

$$\mathbf{n} = \frac{1}{\sqrt{1+\nabla_y\eta^2}}\begin{pmatrix}1\\-\nabla_y\eta\end{pmatrix} \tag{6}$$

so that the continuity condition for the heat flow can be reduced to

$$[\lambda(\partial_x T - \nabla_y\eta\,.\,\nabla_y T)]_\eta = 0. \tag{7}$$

Collecting the terms of Eqs. (5) and (7) with the same powers of δ then provides the jump conditions for the perturbations T_j of the temperature.

It is convenient for the linear and WNL regimes to consider the Fourier modes of the interface

$$\eta(t,\mathbf{y}) = \int d^2\mathbf{k}\,\exp(i\mathbf{k}\cdot\mathbf{y})\,\hat{\eta}(t,\mathbf{k}).$$

In this paper we first address the single-mode case

$$\eta_0(\mathbf{y}) = \delta\cos(\mathbf{k}_p\cdot\mathbf{y}), \tag{8}$$

which reads in the Fourier domain as

$$\hat{\eta}_0(\mathbf{k}) = (\delta/2)[\delta_0(\mathbf{k}-\mathbf{k}_p) + \delta_0(\mathbf{k}+\mathbf{k}_p)], \tag{9}$$

where δ_0 is the Dirac function at 0. We then focus our attention to the multimode case. We model the initial perturbation $\eta_0(\mathbf{y})$ of the interface elevation as the realization of a spatially random process with Gaussian statistics. The statistical distribution of this process is characterized by the first two moments

$$\langle\eta_0(\mathbf{y})\rangle = 0, \quad \langle\eta_0(\mathbf{y})\,\eta_0(\mathbf{y}')\rangle = C_0(\mathbf{y}-\mathbf{y}'),$$

where the brackets stand for a statistical average and C_0 is the so-called autocorrelation function. An equivalent definition of the random process in terms of Fourier modes is that $\hat{\eta}_0(\mathbf{k})$ has Gaussian statistics characterized by

$$\langle\hat{\eta}_0(\mathbf{k})\rangle = 0, \quad \langle\hat{\eta}_0(\mathbf{k})\,\hat{\eta}_0(\mathbf{k}')\rangle = \Gamma_0(\mathbf{k})\,\delta_0(\mathbf{k}+\mathbf{k}'),$$

where $\Gamma_0(\mathbf{k})$ is the so-called power spectral density (PSD). As shown in Ref. 13 the PSD is proportional to the Fourier transform of the autocorrelation function. A limit case is the white noise model where the correlation radius of the process is assumed to be very small. The autocorrelation function is then reduced to a Dirac distribution $C_0(\mathbf{y})=\sigma_0^2\delta_0(\mathbf{y})$ and the PSD is identically equal to the constant $\sigma_0^2/(2\pi)^2$. Please note that σ_0 is not a rms, but σ_0^2 has the dimension of a length to the power 4.

The choice of a statistical description for the multimode interface is both mathematically and physically relevant. Indeed the initial modulation of the surface is only known approximatively. The statistical model takes into account the available data (rms, spectrum) and completes the unknown data by putting a statistical distribution on them. This distri-

bution should be chosen in a natural way, and the most natural model (maximizing the entropy) when only the first two moments are specified is the Gaussian statistics. Finally, the choice of the Gaussian statistics is also consistent with the empirical picture that the initial interface perturbation originates from many small imperfections: we can then invoke the central limit theorem which claims that the Gaussian statistics always results from the contribution of many independent effects.

Before introducing the equations governing the dynamics, we would like to comment on the interpretation of the results. We consider a set of possible realizations of the initial perturbation of the interface. From a practical point of view we seek information which holds true for an arbitrary realization of the interface. We are going to perform calculations to compute statistical averages. Throughout the paper we focus our attention to the PSD of the modulation. This function actually contains all the information about the spatial process η. The ergodic principle gives the equivalence between the theoretical statistical average and the experimental local or global spatial averages, such as the spatial spectrum or the rms. It is equivalent to compute a statistical average over all possible realizations in a fixed point and to compute a spatial average for an arbitrary realization. Actually, the statistical theory provides accurate results depending only on the autocorrelation function. For instance, the local shape of a local maximum can be computed theoretically, as well as the density of local maxima above a given value, etc. (see, for instance, Ref. 13).

III. SINGLE-MODE PERTURBATION

We first address the case of a single-mode initial disturbance with wave number $\mathbf{k}$: $\eta(t=0,\mathbf{y})=\delta\cos(\mathbf{k}\cdot\mathbf{y})$. The linear stability analysis establishes that in the early steps of the dynamics the interface modulation is single mode and grows exponentially in time with the characteristic growth rate $\gamma(\mathbf{k})$.[14] The WNL analysis exhibits mode coupling that drives up harmonic modes.[15] The WNL problem is reduced to the identification of a finite set of Fourier coefficients

$$\hat{\eta}(t,\mathbf{k}) = \delta\hat{\eta}_1(t,\mathbf{k}) + \delta^3\hat{\eta}_3(t,\mathbf{k}),$$

$$\hat{\eta}(t,2\mathbf{k}) = \delta^2\hat{\eta}_2(t,2\mathbf{k}),$$

$$\hat{\eta}(t,3\mathbf{k}) = \delta^3\hat{\eta}_3(t,3\mathbf{k}).$$

Here $\hat{\eta}_1$ is given by the linear stability analysis. The term $\hat{\eta}_2(t,2\mathbf{k})$ originates from a second-order WNL effect (second-harmonic generation). Calculations show that there is no excitation of a zeroth harmonic in the sense that $\hat{\eta}(t,0\mathbf{k})$ is vanishing. The term $\hat{\eta}_3(t,3\mathbf{k})$ originates from a third-order WNL effect (third-harmonic generation). The third-order WNL term $\hat{\eta}_3(t,\mathbf{k})$ gives the nonlinear correction to the exponential growth of the fundamental modulation.

A. Linear stability analysis

The linear stability analysis shows the existence of four possible linear modes for the hydrodynamic variables U_1 (one sonic mode in the overdense region, one sonic mode which merges with a thermal conduction mode, and two vorticity modes in the blowoff region).[9] The amplitudes of the modes are four free parameters. They can be expressed in terms of the modulation interface η_1 by the four linearized jump conditions satisfied by the hydrodynamic variables at the interface. It is necessary to exhibit one more relation to fix the growth rate. This relation is obtained by studying the thermal flow. T_1 consists of five modes which depend on the hydrodynamic parameters and two more free parameters. The jump conditions for the temperature and the heat flow read as three complicated relations that can be dramatically simplified by using a separation of scales technique based on the assumption $d_L|\mathbf{k}|\ll 1\ll d_R|\mathbf{k}|$. Accordingly, the two free parameters of T_1 are eliminated, and a new relation is established between the parameter of the sonic mode of the blowoff region and η_1. This provides a compatibility condition for the instability growth rate γ that does not depend on the values of the thermal diffusion lengths,

$$\gamma(\mathbf{k}) = \sqrt{Ag|\mathbf{k}| - |\mathbf{k}|^2 u_L u_R A^2} - (1+A)|\mathbf{k}|u_L, \tag{10}$$

where $u_L=\dot{m}/\rho_L$ (resp. $u_R=\dot{m}/\rho_R$) is the ablation velocity (resp. blowoff velocity), and $A=(\rho_L-\rho_R)/(\rho_R+\rho_L)=(u_R-u_L)/(u_R+u_L)$ is the Atwood number. Note that the expression of the growth rate γ is in complete agreement with the one derived in Ref. 9. γ is positive for any wave number below the cutoff wave number $k_c=g/(u_L u_R)\times(u_R-u_L)/(u_L+u_R)$. γ is maximal for a modulation with wave number

$$k_{\mathrm{opt}} = \frac{g}{2u_L u_R}\frac{\sqrt{u_R}-\sqrt{u_L}}{\sqrt{u_L}+\sqrt{u_R}}. \tag{11}$$

If $|\mathbf{k}|\ll k_{\mathrm{opt}}$, then we get the classical RT growth rate $\gamma(\mathbf{k})=\sqrt{Ag|\mathbf{k}|}$.

B. Second-order weakly nonlinear regime

The second-order WNL analysis consists in collecting the terms of order δ^2 in the system of conservation laws and in the jump conditions for the hydrodynamic variables and the temperature. As shown in the Appendix the system of conservation laws provides a system of linear equations for the hydrodynamic variables U_2 with source terms which are quadratic functions of the first-order perturbations U_1. This system is solved in Ref. 16 with the use of a symbolic maniupulator program (maple). The existence of five hydrodynamic modes with four free parameters is derived. In particular, there is no vorticity mode in the overdense region, while vorticity plays an important role in the blowoff region. The four free parameters of U_2 can be related to η_2 by the four jump conditions that also read as linear relations between U_2 and η_2 with quadratic source terms in U_1 and η_1. T_2 consists of seven modes containing two free parameters. The jump conditions for the temperature and the heat flow read as three linear relations in terms of T_2 with source terms depending on T_1, U_1, and η_1. Accordingly, the two free parameters of T_2 can be eliminated, and a compatibility condition for η_2 can be obtained. If $|\mathbf{k}|\ll k_{\mathrm{opt}}$, then $\hat{\eta}_2(2\mathbf{k})\simeq A|\mathbf{k}|\hat{\eta}_1^2$. This result is consistent with those obtained in the framework of incompressible, inviscid, irrotational, and immiscible fluids.[15,17] If $|\mathbf{k}|=k_{\mathrm{opt}}$, then

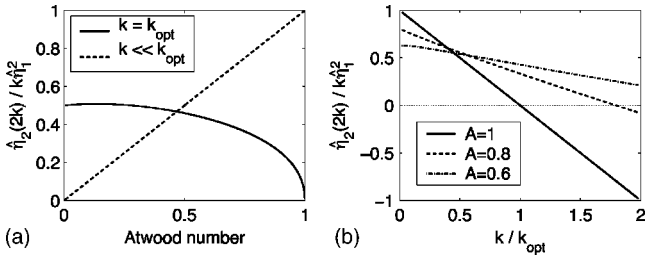

FIG. 2. SHG efficiency $\hat{\eta}_2(2\mathbf{k})$ divided by $\hat{\eta}_1^2|\mathbf{k}|$ as a function of A (a) and $|\mathbf{k}|/k_{\mathrm{opt}}$ (b).

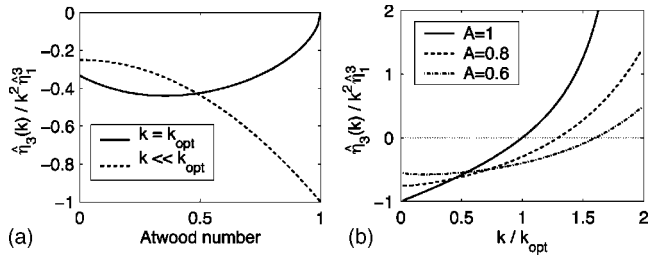

FIG. 3. Nonlinear correction $\hat{\eta}_3(\mathbf{k})$ divided by $\hat{\eta}_1^3|\mathbf{k}|^2$ as a function of A (a) and $|\mathbf{k}|/k_{\mathrm{opt}}$ (b).

$$\hat{\eta}_2(2k_{\mathrm{opt}}) = 2\hat{\eta}_1^2 k_{\mathrm{opt}} \frac{2\sqrt{1-A^2}-1+A}{\sqrt{1-A^2}+3+3A}. \tag{12}$$

If $|\mathbf{k}|$ is of the order of k_{opt}, then Eq. (10) shows that ablation reduces the linear growth rate, while Eq. (12) establishes that it also strongly modifies the second-harmonic generation (SHG) efficiency. This feature is in dramatic contrast with the case of a classical RT system with surface tension. In that case the SHG efficiency is not affected by surface tension and it is equal to the classical efficiency $A|\mathbf{k}|\hat{\eta}_1^2$.[17]

More generally, $\hat{\eta}_2(2\mathbf{k})/(\hat{\eta}_1^2|\mathbf{k}|)$ is a function of A and $|\mathbf{k}|/k_{\mathrm{opt}}$ only. If $A \simeq 1$ then

$$\hat{\eta}_2(2\mathbf{k}) \simeq \hat{\eta}_1^2|\mathbf{k}|(1-|\mathbf{k}|/k_{\mathrm{opt}}) \tag{13}$$

for $|\mathbf{k}| < k_c$. Note that $k_c \simeq 2k_{\mathrm{opt}}$ for $A \simeq 1$. The sign of the SHG efficiency changes when going from $|\mathbf{k}| < k_{\mathrm{opt}}$ to $|\mathbf{k}| > k_{\mathrm{opt}}$. This involves an inversion of the bubble-spike asymmetry. This inversion has recently been described in Ref. 6 in a self-consistent approach where ρ_R is substituted for a $|\mathbf{k}|$-dependent ρ_{k} that is assumed to be $\ll \rho_L$. Figure 2(b) shows that, if $A<1$, then the inversion occurs for some $|\mathbf{k}| > k_{\mathrm{opt}}$.

The analysis of the second-order WNL regime is completed by adding that there is no zeroth-harmonic generation for the modulation interface, but the pressure and the temperature have zeroth-harmonic components.

C. Third-order weakly nonlinear regime

The third-order WNL analysis follows the same lines as the second-order analysis. We get linear systems for the third-order perturbations U_3, η_3, and T_3 in which source terms depending on the first-order and second-order perturbations are coming. On the one hand, it appears that the hydrodynamics is rather simple in the overdense region (no vorticity mode), while it is complicated in the blowoff region. On the other hand, the thermal transport is simple in the blowoff region, but complicated in the overdense region with the existence of a thin boundary layer.

The third-order WNL modes for a single-mode perturbation contains Fourier coefficients at the fundamental frequency and at the third-harmonic frequency. The evolution equations for the WNL correction to the fundamental mode give expressions for U_3 and T_3 containing six free parameters, and we are able to write seven jump relations depending also on $\hat{\eta}_3(\mathbf{k})$. This consequently establishes the expression of $\hat{\eta}_3(\mathbf{k})$. If $|\mathbf{k}| \ll k_{\mathrm{opt}}$ then $\hat{\eta}_3(\mathbf{k}) \simeq -[(1+3A^2)/4]|\mathbf{k}|^2\hat{\eta}_1^3$, which is the same expression as the one derived in Ref. 17 for the dynamics of the interface of two incompressible, inviscid, irrotational, and immiscible liquids. This observation, together with the corresponding one for SHG, shows that our model could be useful to extend the saturation formulas of Haan[18] which are based on these simplified models. Note that, if $\hat{\eta}_1$ is complex valued, then the factor $\hat{\eta}_1^3$ should be replaced by $|\hat{\eta}_1|^2\hat{\eta}_1$ because it is the product $\hat{\eta}_1(\mathbf{k})\hat{\eta}_1(\mathbf{k}) \times \hat{\eta}_1(-\mathbf{k})$ and $\hat{\eta}_1(-\mathbf{k}) = \hat{\eta}_1(\mathbf{k})^*$.

If $|\mathbf{k}| = k_{\mathrm{opt}}$, then $\hat{\eta}_3(k_{\mathrm{opt}}) = \hat{\eta}_1^3 k_{\mathrm{opt}}^2 f(A)$. The function f is plotted in Fig. 3(a). For $A \simeq 1$ it can be expanded as $f(A) \simeq -(2/3)\sqrt{1-A}$. Note that f is negative valued, which shows that the nonlinear correction helps reducing the exponential growth of the fundamental modulation.

More generally, the expression of $\hat{\eta}_3(\mathbf{k})/(\hat{\eta}_1^3|\mathbf{k}|^2)$ is a function of A and $|\mathbf{k}|/k_{\mathrm{opt}}$. If $A \simeq 1$, then the expression of $\hat{\eta}_3(\mathbf{k})$ can be simplified into

$$\hat{\eta}_3(\mathbf{k}) \simeq -\hat{\eta}_1^3|\mathbf{k}|^2 \frac{(4-|\mathbf{k}|/k_{\mathrm{opt}})(1-|\mathbf{k}|/k_{\mathrm{opt}})}{(4-2|\mathbf{k}|/k_{\mathrm{opt}})} \tag{14}$$

for $|\mathbf{k}| < k_c \simeq 2k_{\mathrm{opt}}$, which shows that the nonlinear correction reduces instability for $|\mathbf{k}| < k_{\mathrm{opt}}$, but enhances instability for $|\mathbf{k}| > k_{\mathrm{opt}}$ as observed in Ref. 6. If $A<1$, then the stabilizing effect is stronger as it concerns a broader band of wave numbers including k_{opt} [Fig. 3(b)]. We can thus state that, if $|\mathbf{k}| \ll k_{\mathrm{opt}}$, then the ablation process plays no role in the linear and WNL regimes. If $|\mathbf{k}|$ is of the order of k_{opt}, then ablative effects have to be taken into account in the linear and WNL regimes.

The third-order WNL corrections also involve third-harmonic generation (THG). Following the same strategy as above, we get the expression of the Fourier coefficient $\hat{\eta}_3(3\mathbf{k})$. If $|\mathbf{k}| \ll k_{\mathrm{opt}}$, then $\hat{\eta}_3(3\mathbf{k}) \simeq (4A^2-1)|\mathbf{k}|^2\hat{\eta}_1^3/2$, in agreement with the result obtained in Ref. 17. If $|\mathbf{k}| = k_{\mathrm{opt}}$, then $\hat{\eta}_3(3k_{\mathrm{opt}}) = \hat{\eta}_1^3 k_{\mathrm{opt}}^2 f_{33}(A)$. The function f_{33} is plotted in Fig. 4(a). More generally, the expression of $\hat{\eta}_3(3\mathbf{k})/(\hat{\eta}_1^3|\mathbf{k}|^2)$ is a function of A and $|\mathbf{k}|/k_{\mathrm{opt}}$. If $A \simeq 1$, then the expression of $\hat{\eta}_3(3\mathbf{k})$ can be simplified into

$$\hat{\eta}_3(3\mathbf{k}) = \frac{1}{2}\hat{\eta}_1^3|\mathbf{k}|^2\left(1-2\frac{|\mathbf{k}|}{k_{\mathrm{opt}}}\right)\left(3-2\frac{|\mathbf{k}|}{k_{\mathrm{opt}}}\right) \tag{15}$$

for $|\mathbf{k}| < k_c \simeq 2k_{\mathrm{opt}}$.

D. Self-consistent analysis

The SBM model is the simplest model for the ablation front. It remains to specify the self-consistent density jump

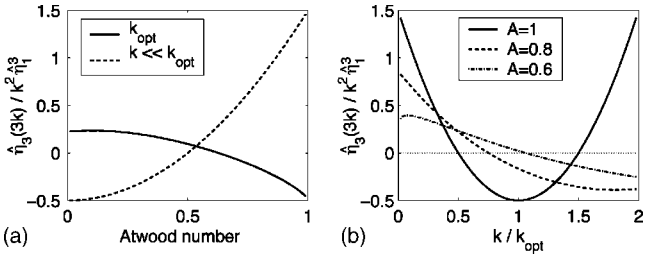

FIG. 4. THG efficiency $\hat{\eta}_3(3\mathbf{k})$ divided by $\hat{\eta}_1^3|\mathbf{k}|^2$ as a function of A (a) and $|\mathbf{k}|/k_{\mathrm{opt}}$ (b).

across the front (or equivalently the Atwood number). This follows from the choice of a corona model for the unperturbed flow and a characteristic length associated with the instability process. The density of the dense region is easy to estimate as the maximum density of the corona. The density of the blowoff plasma can be calculated by a measure of the density at a distance x^* from the front. The expression for the density profile can be obtained from a simple corona model $\rho(x)=\rho_L(nx/d_L)^{1/n}$, $x>0$, where n is the Spitzer exponent of the thermal conductivity $\lambda=\kappa T^n$.[4,8] Since we are dealing with surface modes that decay as $\exp(-|\mathbf{k}|x)$, the characteristic length used to calculate the density must be of the order of $|\mathbf{k}|^{-1}$. According to the results of Refs. 3, 19, and 20, excellent agreement with numerical simulations by Kull[21] in the linear regime is obtained by taking $x^*=1/(2|\mathbf{k}|)$ which gives the jump density $\rho_R=\rho_L(2|\mathbf{k}|d_L/n)^{1/n}$. Note that $|\mathbf{k}|d_L$ has been assumed to be small in the SBM analysis which implies that $\rho_R \ll \rho_L$. All the previous quantities are functions of the Atwood number A and the wave number $\mathbf{k}$, it remains to substitute the self-consistent $A(\mathbf{k})$ to get the desired results. Let us first address the linear regime and derive the expression of the growth rate which reads

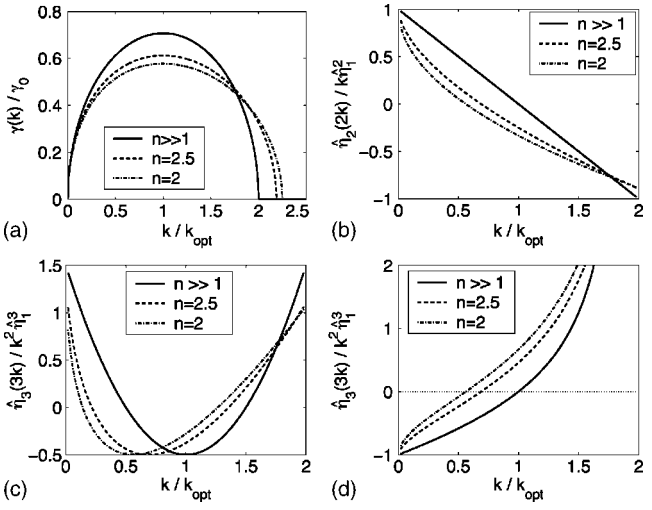

FIG. 5. Growth rate $\gamma(\mathbf{k})$ divided by $\gamma_0=\sqrt{gk_{\mathrm{opt}}}$ (a), SHG efficiency $\hat{\eta}_2(2\mathbf{k})$ divided by $\hat{\eta}_1^2|\mathbf{k}|$ (b), THG efficiency $\hat{\eta}_3(3\mathbf{k})$ divided by $\hat{\eta}_1^3|\mathbf{k}|^2$ (c), nonlinear correction $\hat{\eta}_3(\mathbf{k})$ divided by $\hat{\eta}_1^3|\mathbf{k}|^2$ (d) as a function of $|\mathbf{k}|/k_{\mathrm{opt}}$. n is the Spitzer exponent.

$$\gamma(\mathbf{k})=\sqrt{gk_{\mathrm{opt}}}\sqrt{\frac{|\mathbf{k}|}{k_{\mathrm{opt}}}-\frac{n}{2n-1}\left(\frac{|\mathbf{k}|}{k_{\mathrm{opt}}}\right)^{2-(1/n)}}, \tag{16}$$

where k_{opt} corresponds to the most instable wave number

$$k_{\mathrm{opt}}=\frac{g}{u_L^2}F_r^{-1/(n-1)}\left(\frac{n}{2n-1}\right)^{n/(n-1)}\left(\frac{2}{n}\right)^{1/(n-1)} \tag{17}$$

and $F_r=u_L^2/(gd_L)$ is the Froude number. Note that the cutoff wave number is $k_c=k_{\mathrm{opt}}(2-1/n)^{n/(n-1)}$. The SHG efficiency for a single-mode perturbation with wave number $\mathbf{k}$ is

$$\hat{\eta}_2(2\mathbf{k})=\hat{\eta}_1^2|\mathbf{k}|[1-c_n(\mathbf{k})], \quad c_n(\mathbf{k})=\frac{2n}{2n-1}\left(\frac{|\mathbf{k}|}{k_{\mathrm{opt}}}\right)^{1-(1/n)}$$

Note that $\hat{\eta}_2(2\mathbf{k})>0$ for $|\mathbf{k}|\ll k_{\mathrm{opt}}$, while $\hat{\eta}_2(2k_{\mathrm{opt}})<0$. This shows the inversion of the bubble-spike asymmetry that has already been obtained in Ref. 6. Similarly the THG efficiency is

$$\hat{\eta}_3(3\mathbf{k})=\tfrac{1}{2}\hat{\eta}_1^3|\mathbf{k}|^2[1-2c_n(\mathbf{k})][3-2c_n(\mathbf{k})].$$

Finally the nonlinear correction to the fundamental modulation is

$$\hat{\eta}_3(\mathbf{k})=-\hat{\eta}_1^3|\mathbf{k}|^2\frac{[4-c_n(\mathbf{k})][1-c_n(\mathbf{k})]}{4-2c_n(\mathbf{k})}.$$

Note that $\hat{\eta}_3(\mathbf{k})/\hat{\eta}_1^3<0$ for $|\mathbf{k}|\ll k_{\mathrm{opt}}$ which shows that modulations with long wavelengths are stabilized by WNL coupling. However $\hat{\eta}_3(k_{\mathrm{opt}})/\hat{\eta}_1^3>0$ which means that the third-order nonlinear correction enhances the instability of the fundamental modulation. This observation can also be found in Ref. 6. However we shall get a very different result in the multimode case.

IV. MULTIMODE PERTURBATION

A. Linear regime

Let us consider an initial multimode disturbance with Gaussian statistics. In the linear regime, the Fourier modes $\hat{\eta}_1$ grow independently from each other. If $\partial_t\hat{\eta}(t=0,\mathbf{k})=0$, then $\hat{\eta}_1(t,\mathbf{k})=\hat{\eta}_0(\mathbf{k})\cosh[\gamma(\mathbf{k})t]$. After a short transition period we have

$$\hat{\eta}_1(t,\mathbf{k})=\tfrac{1}{2}\hat{\eta}_0(\mathbf{k})\exp[\gamma(\mathbf{k})t] \tag{18}$$

so that the PSD is

$$\Gamma_{\mathrm{lin}}(t,\mathbf{k})=\tfrac{1}{4}\Gamma_0(\mathbf{k})\exp[2\gamma(\mathbf{k})t]. \tag{19}$$

The gain curve has a maximum at k_{opt}. If the initial modulation is broadband $\Gamma_0(\mathbf{k})\simeq\Gamma_0$, and if $\gamma(k_{\mathrm{opt}})t>1$, then the PSD is a Gaussian curve centered at k_{opt},

$$\Gamma_{\mathrm{lin}}(t,\mathbf{k})\simeq\frac{1}{4}\Gamma_0\exp[2\gamma(k_{\mathrm{opt}})t]\exp\left(-\frac{(|\mathbf{k}|-k_{\mathrm{opt}})^2}{k_t^2}\right).$$

Note that the width $k_t=k_{\mathrm{opt}}/\sqrt{\gamma(k_{\mathrm{opt}})t}$ decays as time increases, which is a manifestation of the spectral gain narrowing effect.

B. Statistical analysis of the nonlinear regime

By computing the third-order correction we get that the Fourier modes of the interface can be expanded as

$$\hat{\eta}(t,\mathbf{k}) = \delta\hat{\eta}_1(t,\mathbf{k}) + \delta^2\hat{\eta}_2(t,\mathbf{k}) + \delta^3\hat{\eta}_3(t,\mathbf{k}) + O(\delta^4),$$

where $\hat{\eta}_1(t,\mathbf{k})$ is the linear mode given by Eq. (18) and $\hat{\eta}_j(t,\mathbf{k}), j=2, 3$, results from all possible combinations of j linear modes,

$$\hat{\eta}_2(t,\mathbf{k}) = \int G_2(\mathbf{k}_1,\mathbf{k}-\mathbf{k}_1)\,\hat{\eta}_1(\mathbf{k}_1)\,\hat{\eta}_1(\mathbf{k}-\mathbf{k}_1)d^2\mathbf{k}_1, \qquad (20)$$

$$\hat{\eta}_3(t,\mathbf{k}) = \int G_3(\mathbf{k}_1,\mathbf{k}_2,\mathbf{k}-\mathbf{k}_1-\mathbf{k}_2)\,\hat{\eta}_1(\mathbf{k}_1)\,\hat{\eta}_1(\mathbf{k}_2) \times \hat{\eta}_1(\mathbf{k}-\mathbf{k}_1-\mathbf{k}_2)d^2\mathbf{k}_1 d^2\mathbf{k}_2, \qquad (21)$$

with G_2 and G_3 being symmetric in their arguments. $G_2(\mathbf{k}_1,\mathbf{k}_2)$ is the sum-frequency generation (SFG) efficiency for the two-mode conversion $\mathbf{k}_1+\mathbf{k}_2$, and $G_3(\mathbf{k}_1,\mathbf{k}_2,\mathbf{k}_3)$ is the SFG efficiency for the three-mode conversion $\mathbf{k}_1+\mathbf{k}_2+\mathbf{k}_3$. Explicit formulas are given in Sec. IV C. The second moment can be expanded as

$$\langle\hat{\eta}(t,\mathbf{k})\,\hat{\eta}(t,\mathbf{k}')^*\rangle = \delta^2\langle\hat{\eta}_1(\mathbf{k})\,\hat{\eta}_1(\mathbf{k}')^*\rangle + \delta^4\langle\hat{\eta}_2(\mathbf{k})\,\hat{\eta}_2(\mathbf{k}')^*\rangle + \delta^4\langle\hat{\eta}_3(\mathbf{k})\,\hat{\eta}_1(\mathbf{k}')^*\rangle + \delta^4\langle\hat{\eta}_1(\mathbf{k})\,\hat{\eta}_3(\mathbf{k}')^*\rangle.$$

Terms of the type $\delta^3\langle\hat{\eta}_2\hat{\eta}_1\rangle$ are vanishing because they only contain odd-order moments of $\hat{\eta}_0$ which is a zero-mean Gaussian process.[13] This equation shows that the lowest-order WNL correction for the PSD depends on the second- and third-order terms of the WNL expansion. That is why it is necessary to develop a third-order WNL analysis to capture the WNL regime in the multimode case. The frequency autocorrelation function then reads

$$\begin{aligned}\langle\hat{\eta}(t,\mathbf{k})\,\hat{\eta}(t,\mathbf{k}')^*\rangle &= \delta^2\langle\hat{\eta}_1(\mathbf{k})\,\hat{\eta}_1(\mathbf{k}')^*\rangle \\ &+ \delta^4\int\int G_2(\mathbf{k}_1,\mathbf{k}-\mathbf{k}_1)G_2(\mathbf{k}_2,\mathbf{k}-\mathbf{k}_2)\langle\hat{\eta}_1(\mathbf{k}_1)\,\hat{\eta}_1(\mathbf{k}-\mathbf{k}_1)\,\hat{\eta}_1(\mathbf{k}_2)^*\,\hat{\eta}_1(\mathbf{k}'-\mathbf{k}_2)^*\rangle d^2\mathbf{k}_1 d^2\mathbf{k}_2 \\ &+ \delta^4\int\int G_3(\mathbf{k}_1,\mathbf{k}_2,\mathbf{k}-\mathbf{k}_1-\mathbf{k}_2)\langle\hat{\eta}_1(\mathbf{k}_1)\,\hat{\eta}_1(\mathbf{k}_2)\,\hat{\eta}_1(\mathbf{k}-\mathbf{k}_1-\mathbf{k}_2)\,\hat{\eta}_1(\mathbf{k}')^*\rangle d^2\mathbf{k}_1 d^2\mathbf{k}_2 \\ &+ \delta^4\int\int G_3(\mathbf{k}_1,\mathbf{k}_2,\mathbf{k}'-\mathbf{k}_1-\mathbf{k}_2)\langle\hat{\eta}_1(\mathbf{k}_1)\,\hat{\eta}_1(\mathbf{k}_2)\,\hat{\eta}_1(\mathbf{k}'-\mathbf{k}_1-\mathbf{k}_2)\,\hat{\eta}_1(\mathbf{k})^*\rangle d^2\mathbf{k}_1 d^2\mathbf{k}_2.\end{aligned}$$

The fluctuations of the interface elevation are initially Gaussian distributed, so that we can express the fourth-order moments as sums of products of second-order moments,[13]

$$\begin{aligned}&\langle\hat{\eta}_0(\mathbf{k}_1)\,\hat{\eta}_0(\mathbf{k}_2)\,\hat{\eta}_0(\mathbf{k}_3)\,\hat{\eta}_0(\mathbf{k}_4)\rangle \\ &\quad= \langle\hat{\eta}_0(\mathbf{k}_1)\,\hat{\eta}_0(\mathbf{k}_2)\rangle\langle\hat{\eta}_0(\mathbf{k}_3)\,\hat{\eta}_0(\mathbf{k}_4)\rangle \\ &\quad\quad+ \langle\hat{\eta}_0(\mathbf{k}_1)\,\hat{\eta}_0(\mathbf{k}_3)\rangle\langle\hat{\eta}_0(\mathbf{k}_2)\,\hat{\eta}_0(\mathbf{k}_4)\rangle \\ &\quad\quad+ \langle\hat{\eta}_0(\mathbf{k}_1)\,\hat{\eta}_0(\mathbf{k}_4)\rangle\langle\hat{\eta}_0(\mathbf{k}_2)\,\hat{\eta}_0(\mathbf{k}_3)\rangle\end{aligned}$$

so that

$$\begin{aligned}&\langle\hat{\eta}_0(\mathbf{k}_1)\,\hat{\eta}_0(\mathbf{k}_2)\,\hat{\eta}_0(\mathbf{k}-\mathbf{k}_1-\mathbf{k}_2)\,\hat{\eta}_0(\mathbf{k}')^*\rangle \\ &\quad= \delta_0(\mathbf{k}_1+\mathbf{k}_2)\,\delta_0(\mathbf{k}-\mathbf{k}')\Gamma_0(\mathbf{k}_1)\Gamma_0(\mathbf{k}) \\ &\quad\quad+ \delta_0(\mathbf{k}-\mathbf{k}_2)\,\delta_0(\mathbf{k}-\mathbf{k}')\Gamma_0(\mathbf{k}_1)\Gamma_0(\mathbf{k}) \\ &\quad\quad+ \delta_0(\mathbf{k}-\mathbf{k}_1)\,\delta_0(\mathbf{k}-\mathbf{k}')\Gamma_0(\mathbf{k}_2)\Gamma_0(\mathbf{k}).\end{aligned}$$

Using Eq. (18) and substituting into the expression of $\langle\hat{\eta}(t,\mathbf{k})\,\hat{\eta}(t,\mathbf{k}')\rangle$ yields $\langle\hat{\eta}(t,\mathbf{k})\,\hat{\eta}(t,\mathbf{k}')^*\rangle = \Gamma(t,\mathbf{k})\,\delta_0(\mathbf{k}-\mathbf{k}')$ where the PSD $\Gamma(t,\mathbf{k})$ is given by

$$\begin{aligned}\Gamma(t,\mathbf{k}) &= \frac{1}{4}\Gamma_0(\mathbf{k})e^{2\gamma(\mathbf{k})t} + \frac{1}{32}\int\overline{G}_2(\mathbf{k}_1,\mathbf{k}-\mathbf{k}_1)^2\Gamma_0(\mathbf{k}_1) \\ &\quad\times\Gamma_0(\mathbf{k}-\mathbf{k}_1)e^{2\gamma(\mathbf{k}_1)t+2\gamma(\mathbf{k}-\mathbf{k}_1)t}d^2\mathbf{k}_1 \\ &\quad+ \frac{1}{16}\int\overline{G}_3(\mathbf{k}_1,\mathbf{k})\Gamma_0(\mathbf{k})\Gamma_0(\mathbf{k}_1)e^{2\gamma(\mathbf{k}_1)t+2\gamma(\mathbf{k})t}d^2\mathbf{k}_1,\end{aligned} \qquad (22)$$

with

$$\overline{G}_2(\mathbf{k}_1,\mathbf{k}_2) = 2G_2(\mathbf{k}_1,\mathbf{k}_2), \quad \overline{G}_3(\mathbf{k}_1,\mathbf{k}_2) = 6G_3(\mathbf{k}_1,-\mathbf{k}_1,\mathbf{k}_2). \qquad (23)$$

The statistical analysis shows that we need only to compute the third-order SFG efficiency for configurations $\mathbf{k}_1-\mathbf{k}_1+\mathbf{k}_2$, and not for all combinations of three modes $\mathbf{k}_1+\mathbf{k}_2+\mathbf{k}_3$. Furthermore, we can distinguish two different types of initial configurations. If the initial spectrum is narrow and contains only short wave numbers $|\mathbf{k}|\ll k_{\text{opt}}$, then we should focus our attention to the computations of $\overline{G}_2(\mathbf{k}_1,\mathbf{k}_2)$ and $\overline{G}_3(\mathbf{k}_1,\mathbf{k}_2)$ for $|\mathbf{k}_j|\ll k_{\text{opt}}$. If the initial spectrum is broad and contains modes with wave numbers $|\mathbf{k}|\sim k_{\text{opt}}$, then the spectral gain enhances these modes during the linear regime, so that they prevail at the early steps of the WNL regime. In such a

configuration, the important quantities to compute are $\overline{G_2}(\mathbf{k}_1,\mathbf{k}_2)$ and $\overline{G_3}(\mathbf{k}_1,\mathbf{k}_2)$ for $|\mathbf{k}_1|\simeq|\mathbf{k}_2|\simeq k_{\text{opt}}$.

C. Sum-frequency generation

The SFG efficiency $\overline{G_2}(\mathbf{k}_1,\mathbf{k}_2)$ for the conversion $\mathbf{k}_1+\mathbf{k}_2$ can be computed by using the same strategy as the one applied for the calculation of the SHG efficiency in the single-mode case, but by considering a bimode initial disturbance,

$$\eta_0(\mathbf{y}) = \delta[\eta_{0,1}\cos(\mathbf{k}_1\cdot\mathbf{y}) + \eta_{0,2}\cos(\mathbf{k}_2\cdot\mathbf{y})]. \tag{24}$$

The second-order WNL corrections then contain a mode with wave number $\mathbf{k}_{12}=\mathbf{k}_1+\mathbf{k}_2$ and amplitude $\delta^2\hat{\eta}_2(\mathbf{k}_{12})$ that can be computed by the same way we have computed $\delta^2\hat{\eta}_2(2\mathbf{k})$ in the single-mode case. By Eqs. (20) and (23) the efficiency $\overline{G_2}(\mathbf{k}_1,\mathbf{k}_2)$ is obtained from the identity

$$\hat{\eta}_2(\mathbf{k}_{12}) = \overline{G_2}(\mathbf{k}_1,\mathbf{k}_2)\,\hat{\eta}_1(\mathbf{k}_1)\,\hat{\eta}_1(\mathbf{k}_2),$$

where $\hat{\eta}_1(\mathbf{k}_j)=\eta_{0j}\exp[\gamma(\mathbf{k}_j)t]/2$. The expression of $\overline{G_2}$ allows a precise description of mode coupling in the multimode spectrum.

If $|\mathbf{k}_1|,|\mathbf{k}_2|\ll k_{\text{opt}}$, then we get the same formula as in Ref. 17, which means that ablation plays no role. If we focus our attention to the conversion configurations with wave numbers $|\mathbf{k}_1|$ and $|\mathbf{k}_2|$ close to k_{opt}, then the SFG efficiency is of the form $\overline{G_2}(\mathbf{k}_1,\mathbf{k}_2)=|\mathbf{k}_{12}|F_{12}(A,|\mathbf{k}_{12}|/k_{\text{opt}})$. For $A\simeq 1$, $\overline{G_2}$ becomes simple:

$$\overline{G_2}(\mathbf{k}_1,\mathbf{k}_2) = |\mathbf{k}_{12}|\frac{(|\mathbf{k}_{12}|/k_{\text{opt}})^2-4}{(|\mathbf{k}_{12}|/k_{\text{opt}})^2-2|\mathbf{k}_{12}|/k_{\text{opt}}+4}. \tag{25}$$

Previous papers have developed mode-coupling formulas based on classical RT systems with surface tension, which is a system much simpler than the ablative RT system. In a second step, these formulas are applied to ablative RT by substitution of the ablative linear growth rate, for instance, the Takabe formula.[15] This approach is interesting in that it gives a first simple estimate of the mode-coupling effects in ablative RT systems. It has been widely applied,[22] especially for the design of ICF targets. Haan has proposed in Ref. 15 a mode-coupling formula that can be applied with an arbitrary dispersion relation $\gamma(\mathbf{k})$. Applying this formula with Eq. (10) for $A=1$ we get

$$\overline{G_H}(\mathbf{k}_1,\mathbf{k}_2) = \frac{|\mathbf{k}_{12}|}{2}\frac{(|\mathbf{k}_{12}|/k_{\text{opt}})^2+4|\mathbf{k}_{12}|/k_{\text{opt}}-8}{(|\mathbf{k}_{12}|/k_{\text{opt}})^2-2|\mathbf{k}_{12}|/k_{\text{opt}}+4}. \tag{26}$$

Comparing with the exact WNL expression (25), we can see that Haan's formula gives a right estimate for the low-frequency modulations, but overestimates high-frequency conversion [Fig. 6(b)].

Let us now compute $\overline{G_3}(\mathbf{k}_1,\mathbf{k}_2)$. For this, we consider the bimode initial disturbance (24) and we look for the expression of the Fourier mode $\hat{\eta}(t,\mathbf{k}_2)$ taking into account all the third-order WNL corrections. We get

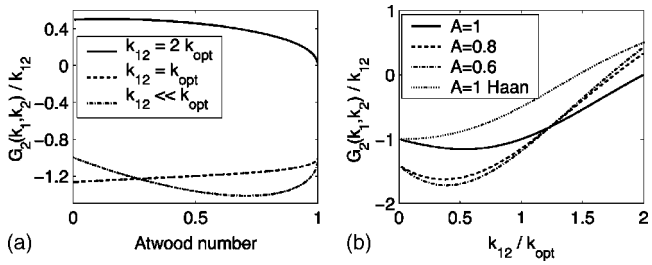

FIG. 6. SFG efficiency $\overline{G_2}(\mathbf{k}_1,\mathbf{k}_2)$ for two wave vectors $\mathbf{k}_1,\mathbf{k}_2$ with wave numbers close to k_{opt}. The dotted line in (b) is based on Haan's mode-coupling formula.

$$\hat{\eta}(t,\mathbf{k}_2) = \delta\hat{\eta}_1(\mathbf{k}_2) + \delta^3\hat{\eta}_{3,1}(\mathbf{k}_2) + \delta^3\hat{\eta}_{3,2}(\mathbf{k}_1,\mathbf{k}_2), \tag{27}$$

where $\hat{\eta}_{3,1}(\mathbf{k}_2)$ is the feedback of mode $\mathbf{k}_2$ on itself. It results from the interaction $\mathbf{k}_2-\mathbf{k}_2+\mathbf{k}_2$ and it is the term computed for the single-mode perturbation. The WNL term $\hat{\eta}_{3,2}(\mathbf{k}_1,\mathbf{k}_2)$ results from the interaction $\mathbf{k}_2+\mathbf{k}_1-\mathbf{k}_1$. By Eqs. (21) and (23) the SFG efficiency $\overline{G_3}$ is obtained from the identity

$$\hat{\eta}_{3,2}(\mathbf{k}_1,\mathbf{k}_2) = \overline{G_3}(\mathbf{k}_1,\mathbf{k}_2)\,\hat{\eta}_1(\mathbf{k}_2)\,\hat{\eta}_1(\mathbf{k}_1)\,\hat{\eta}_1(-\mathbf{k}_1).$$

If $|\mathbf{k}_1|\sim|\mathbf{k}_2|\ll k_{\text{opt}}$, then

$$\overline{G_3}(\mathbf{k}_1,\mathbf{k}_2) = |\mathbf{k}_2|^2F_3(A,\theta). \tag{28}$$

Here F_3 is a function that depends only on the Atwood number A and the angle θ between the wave vectors $\mathbf{k}_1$ and $\mathbf{k}_2$:

$$F_3(A,\theta) = A^2[F_{3,1}(c_\theta)+F_{3,1}(s_\theta)] + [F_{3,2}(c_\theta)+F_{3,2}(s_\theta)], \tag{29}$$

where $c_\theta=|\cos(\theta/2)|$, $s_\theta=|\sin(\theta/2)|$, $F_{3,1}(c)=c(2-2c+3c)(2-2c-c^2)$, and $F_{3,2}(c)=\frac{1}{4}(-3+8c^2-4c^3)$. If $|\mathbf{k}_1|\sim|\mathbf{k}_2|\sim k_{\text{opt}}$, then $\overline{G_3}$ is still given by Eq. (28), where F_3 is a complicated function that depends only on A and θ. In particular, if $A\simeq 1$, then

$$F_3(A,\theta) \simeq -\sin(\theta)^2\frac{\sqrt{2}-1}{\sqrt{1-A}}, \tag{30}$$

which is negative valued for any θ. This shows that the WNL term $\hat{\eta}_{3,2}(\mathbf{k}_1,\mathbf{k}_2)$ in Eq. (27) helps reducing the exponential growth of the mode $\mathbf{k}_2$. In the case of a bimode initial disturbance with wave numbers close to k_{opt}, the total third-order WNL term is the sum of the feedback term $\hat{\eta}_{3,1}(\mathbf{k}_2)$ that can be destabilizing (see Sec. III C) and of the stabiliz-

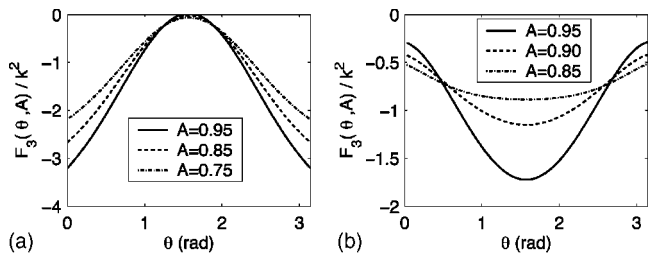

FIG. 7. Function F_3 describing the nonlinear feedback of modes $\mathbf{k}_1$ and $-\mathbf{k}_1$ on mode $\mathbf{k}$, in the case $|\mathbf{k}|\sim|\mathbf{k}_1|\ll k_{\text{opt}}$ (a) and in the case $|\mathbf{k}|\sim|\mathbf{k}_1|\sim k_{\text{opt}}$ (b). θ is the angle between $\mathbf{k}$ and $\mathbf{k}_1$.

ing term $\hat{\eta}_{3,2}(\mathbf{k}_1,\mathbf{k}_2)$. The total WNL effect can thus be stabilizing or destabilizing depending on the initial values of $\eta_{0,1}$ and $\eta_{0,2}$, the wave numbers and the Atwood number. In the following we consider a continuous spectrum. In this case the WNL term $\hat{\eta}_{3,1}(\mathbf{k}_2)$ which results from the interaction $\mathbf{k}_2+\mathbf{k}_2-\mathbf{k}_2$ is negliglible compared to the sum of the numerous contributions $\hat{\eta}_{3,2}(\mathbf{k}_1,\mathbf{k}_2)$ which result from the interactions $\mathbf{k}_2+\mathbf{k}_1-\mathbf{k}_1$ with all the linear modes $\mathbf{k}_1$. Consequently the total third-order WNL term in the multimode case is always stabilizing. The following section is devoted to a quantitative analysis of the WNL stabilization.

D. Saturation amplitude

Let us assume that the initial spectrum is narrow band with a typical wave number $k_0 \ll k_{\text{opt}}$. Integrating Eq. (22) yields that the nonlinear feedback to the fundamental modulations reduces the exponential growth

$$\Gamma(t,\mathbf{k}) = \Gamma_{\text{lin}}(t,\mathbf{k})[1 + |\mathbf{k}|^2 f_3(A)\text{rms}^2_{\text{lin}}(t)], \tag{31}$$

where rms_{lin} is the interface elevation rms computed in the linear regime $[\text{rms}^2_{\text{lin}}(t)=\int\Gamma_{\text{lin}}(t,\mathbf{k})d^2\mathbf{k}]$ and $f_3(A)\simeq -0.17 - 0.58A^2$. If the initial spectrum is broadband, then the prevailing modes in the early steps of the WNL regime are the ones around k_{opt} by spectral gain narrowing. If $|\mathbf{k}|\sim k_{\text{opt}}$, then the PSD reads as Eq. (31) with $f_3(A)\simeq -(\sqrt{2}-1)/(2\sqrt{1-A})$ if $A\simeq 1$. The sign of $f_3(A)<0$ shows that the nonlinear correction slows down the exponential growth of the fundamental modulations. The saturation occurs when the growth of one of the modes is stopped. At this time $\text{rms}_{\text{lin}} \sim \lambda/(2\pi\sqrt{2|f_3(A)|})$, or in terms of the local rms

$$\text{rms}_{\text{loc}}(t) = \int_{0.75k_0\leqslant|\mathbf{k}|\leqslant 1.25k_0} \Gamma(t,\mathbf{k})d^2\mathbf{k}$$

the saturation amplitude is $\text{rms}_{\text{loc}}\sim\lambda_0/(4\pi\sqrt{|f_3(A)|})$. For long wavelengths and $A\simeq 1$ the saturation amplitude is $\text{rms}_{\text{loc}}\sim 0.09\lambda_0$. A similar formula has been proposed by Haan.[18] He was the first one to suggest that neighboring modes with similar wavelengths add up to create an effective local amplitude, and that nonlinear saturation should occur when this collective amplitude reaches some value $c_{\text{sat}}\lambda$. Haan has fixed the constant c_{sat} by comparisons with numerical simulations. The literature contains a lot of references for the value of c_{sat} for an Atwood number $A=1$,[22–25] which are in the range 0.06–0.1. The statistical WNL analysis allows us to recover analytically the form of the equation that characterizes nonlinear saturation, as well as the value of the constant $c_{\text{sat}}\simeq 0.09$ for $A=1$.

E. Self-consistent analysis

The self-consistent analysis in the multimode case is not as simple as in the single-mode case. The principle is still to specify a self-consistent value for the density of the blowoff plasma. This value is taken from the corona model at some distance from the front corresponding to the spatial extent of the surface modes. The choice of this distance is the key issue. Consider, for instance, the sum-frequency generation $\mathbf{k}_1+\mathbf{k}_2\mapsto\mathbf{k}_{12}$. The computation of the self-consistent value of the SFG efficiency $\overline{G_2}(\mathbf{k}_1,\mathbf{k}_2)$ cannot be reduced to the substitution of a unique effective value of the Atwood number into the previously determined $\overline{G_2}$. Indeed, some of the modes with the wave vector $\mathbf{k}_{12}$ decay as $\exp[-(|\mathbf{k}_1|+|\mathbf{k}_2|)x]$, and some other decay as $\exp(-|\mathbf{k}_{12}|x)$, and thus they do not probe the blowoff plasma at the same depth. For each generated mode the value of the density should be taken as $\rho_R=\rho_L(2kd_L/n)^{1/n}$ with the suitable value for k (that is, $k=|\mathbf{k}_1|+|\mathbf{k}_{12}|$ for the first type of modes, and $|\mathbf{k}_{12}|$ for the second type). This method should be used as well to choose for each generated mode the correct value of the thermal diffusion length $d_R\sim\rho_R^{-n}$. Applying this method we get the SFG efficiency. If both $|\mathbf{k}_1|$ and $|\mathbf{k}_2|$ are smaller than k_{opt}, then ablation plays no role and the standard formula[17] can be applied. The interesting case corresponds to two wave numbers $|\mathbf{k}_j|\sim k_{\text{opt}}$. Figure 8 shows that the SFG efficiency is larger (in absolute value) than the efficiency predicted by Eq. (26). In particular, the generation of long-wavelength modulations $|\mathbf{k}_{12}|\ll k_{\text{opt}}$ is strongly enhanced as pointed out in Ref. 6.

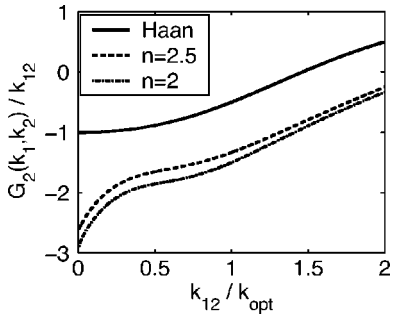

FIG. 8. Self-consistent SFG efficiency in the case $|\mathbf{k}_1|\sim|\mathbf{k}_2|\sim k_{\text{opt}}$ compared with Haan's formula (26).

The computation of the feedbacks to the fundamental modulations can be computed as well. If $|\mathbf{k}|\sim|\mathbf{k}_1|\ll k_{\text{opt}}$, then $\overline{G_3}$ is still given by Eqs. (28) and (29), and if $|\mathbf{k}|\sim|\mathbf{k}_1|\sim k_{\text{opt}}$, then

$$\overline{G_3}(\mathbf{k},\mathbf{k}_1) \simeq -\frac{|\mathbf{k}|^{3/2}}{\sqrt{d_L F_r}} c(n)\sin^2(\theta),$$

where $c(n)$ depends only on n (see Fig. 9). In particular, $c(5/2)\simeq 0.3$.

In the case of an initially narrow-band disturbance with typical long-wavelength λ_0, the saturation amplitude

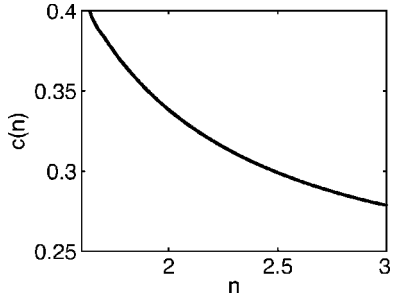

FIG. 9. Parameter $c(n)$ as a function of the Spitzer exponent.

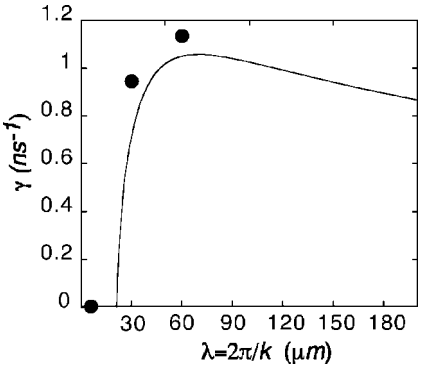

FIG. 10. Linear growth rate spectrum (growth rate vs wavelength) from the results of the 2D FCI2 simulations (dots), and from the linear theory Eq. (10) (solid line).

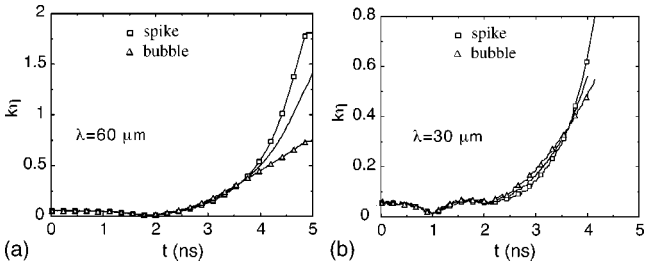

FIG. 11. Time variation of the product of the wave number with the spike amplitude (square), the bubble amplitude (triangle), and the peak-to-valley half amplitude of the ablation front (solid line) with $k\eta_0=6\times10^{-2}$ for (a) 60 μm and (b) 30 μm up to the WNL regime.

$\mathrm{rms}_{\mathrm{loc}}(t)\sim 0.09\lambda_0$. In case of a broadband disturbance the spectral gain enhances modes around k_{opt} and the saturation is effective when

$$\mathrm{rms}_{\mathrm{loc}}(t)\sim \frac{\sqrt[4]{k_{\mathrm{opt}}d_L F_r}}{2\pi\sqrt{2c(n)}}\lambda_{\mathrm{opt}}. \tag{32}$$

In the case of a broadband pulse, we need to specify the parameters of the unperturbed flow. We apply our results in a typical ICF configuration[6] $d_L=0.04$ μm, $n=2.1$, $u_L=3.3$ μm/ns, $g=60$ μm/ns^2. We have $F_r=4.5$, $\lambda_{\mathrm{opt}}=10$ μm, and the saturation amplitude is $\mathrm{rms}_{\mathrm{loc}}(t)\simeq 0.11\lambda_{\mathrm{opt}}$. If we consider a different configuration with a shorter optimal wavelength, such as $d_L=0.2$ μm, then $F_r=1$, $\lambda_{\mathrm{opt}}=2.4$ μm, and $\mathrm{rms}_{\mathrm{loc}}(t)\simeq 0.17\lambda_{\mathrm{opt}}$.

V. NUMERICAL SIMULATIONS

In this section we compare the model predictions with the results of simulations performed with the two-dimensional (2D) Lagrangian code FCI2.[26] We consider a planar 80 μm thick CHOBr foil irradiated by a constant and uniform x-ray flux of 3×10^{13} W/cm^2. After a transient period of 2.3 ns during which the ablation front oscillates (see Fig. 11), the rarefraction wave breaks out at the ablation front and the foil starts to accelerate with the average acceleration $g\simeq 45$ μm/ns^2 and the average ablation velocity $u_L\simeq 3.1$ μm/ns. The ablation front is numerically determined as the location of the density maximum. It could be defined as well as the location of the maximum of the density gradient length scale without significant modification of the numerical results. The density jumps is assessed from the ratio of the density at the ablation front to the density calculated at a distance of $1/(2k)$ from this ablation front $[\rho_L/\rho_R=(n/\rho_k d_L)^{1/n}]$. We obtain, respectively, for 60 and 30 μm, $\rho_L/\rho_R\simeq 17.5$ and $\rho_L/\rho_R\simeq 14.6$ leading to $A\simeq 0.9$.

First of all, results from the model and from the simulations are compared in the linear regime. To ensure that the simulations remain in the linear regime, the product of the wave number with the initial front-surface amplitude $k\eta_0$ is taken as low as 10^{-3}. In Fig. 10, a good agreement is shown between the variations of the linear growth rates as a function of the wavelength, obtained on the one hand from the numerical simulations (dots) and on the other hand from Eq. (10) (solid line).

As illustrated, we managed to perform one simulation with a wave number ($\lambda=6$ μm) greater than the cuttoff wave number predicted by the linear theory ($\lambda_*\simeq 22$ μm). In this case the ablation front amplitude does not grow but it oscillates even after the break out of the rarefraction wave. In the limit of a wavelength larger than the foil thickness the linear theory does not apply. Indeed in this case the boundary effects affect the exponential growth of the linear regime.[27] Accordingly, simulations have been performed only for wavelengths smaller than 80 μm.

The initial front-surface amplitude η_0 was varied in order to probe different growth regimes. The nonlinear regime can be observed with $k\eta_0=6\times10^{-2}$ in Fig. 11 where the time variation of the product of the wave number with the spike amplitude (square), the bubble amplitude (triangle), and the peak-to-valley half amplitude of the ablation front (solid line) are plotted for (a) 60 μm and (b) 30 μm. During the transient period ($0<t<2.3$ ns) the ablation front appears to oscillate. In the 30 μm case the period is approximatively half the 60 μm case in agreement with Ref. 28. The value of this period ($\sim$2.3 ns) is in agreement with the theoretical prediction $T_{30\,\mu\mathrm{m}}=2\pi/\omega_{30\,\mu\mathrm{m}}=2\pi(ku_L\sqrt{\rho_L/\rho_R})^{-1}\simeq 2.5$ ns. As predicted by the theory discussed in this paper and as previously noticed by Sanz *et al.*,[6] the inversion of the bubble-spike asymmetry in the early stage of growth ($2.3<t<3.5$ ns) is exhibited in Fig. 11. Indeed in this stage the bubble amplitude is greater than the spike one. We can also observe that this inversion is more apparent for 30 μm($k>k_{\mathrm{opt}}$) than for 60 μm($k\simeq k_{\mathrm{opt}}$) in agreement with the theory that predicts that the SHG efficiency is proportional to ($k_{\mathrm{opt}}-k$) for $A\simeq 1$ [see Eq. (13)].

Figure 12 shows the enhancement of the ablation front instability by the third-order nonlinear correction in the WNL regime with respect to the linear regime. The linear results which are plotted correspond to the numerical fits ($ae^{\gamma t}+be^{-\gamma t}$) starting at 2.3 ns and multiplied by the ratio of the initial amplitudes, where the growth rate γ is obtained from the numerical results reported in Fig. 10. The theory predicts that the WNL correction to the fundamental mode is proportional to ($k-k_{\mathrm{opt}}$) for $A\simeq 1$ [see Eq. (14)]. This prediction is confirmed by the simulations which show that the

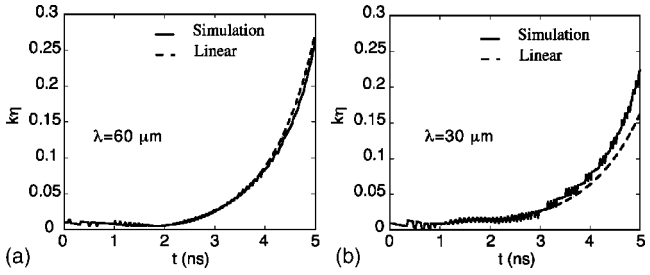

FIG. 12. Time variation of the product of the wave number with the peak-to-valley half amplitude of the ablation front with $k\eta_0=10^{-2}$ for (a) 60 μm and (b) 30 μm from the 2D FCI2 simulations (solid lines), up to the WNL regime, and the linear results (dashed lines). Oscillations superimposed on the curves are numerical artefacts.

WNL feedback enhances the instability with respect to the linear regime for 30 μm and produces no effect for 60 μm.

VI. CONCLUSION

To conclude, the analytical formulas that we have derived show the influence of ablation on RT instability in the linear and WNL regimes. The statistical analysis of the multimode case has allowed us to derive simple expression for the saturation amplitude giving the threshold value for the local rms which corresponds to the WNL stabilization of the exponential growth of the modulations. The limit of large wavelength $\mathrm{rms}_{\mathrm{loc}}\sim 0.1\lambda$ is in agreement with previously known results derived by Haan. The case of short wavelengths in the ablative regime is more interesting, in that we have shown that the saturation amplitude is above Haan's prediction. This shows that ablation reduces the linear growth rate, but it also increases the duration of the linear phase.

ACKNOWLEDGMENTS

The authors thank C. Cherfils-Clérouin and P.-A. Raviart for useful and stimulating discussions.

APPENDIX: EXPANSIONS OF SOLUTIONS OF NONLINEAR HYPERBOLIC SYSTEMS

In this appendix we report and extend the results presented in Ref. 29. We consider a system of conservation laws,

$$\partial_t[\mathbf{h}(\mathbf{U})]+\partial_x[\mathbf{f}(\mathbf{U})]+\sum_{j=1}^{d}\partial_{y_j}[\mathbf{g}_j(\mathbf{U})]=\mathbf{s}(\mathbf{U}), \tag{A1}$$

where x [resp. $\mathbf{y}=(y_j)_{j=1,\ldots,d}$] stands for the longitudinal (resp. transverse) spatial variables. We first consider a one-dimensional solution

$$\partial_t[\mathbf{h}(\mathbf{U}_0)]+\partial_x[\mathbf{f}(\mathbf{U}_0)]=\mathbf{s}(\mathbf{U}_0),\quad \mathbf{U}_0(t=0,x)=\mathbf{U}_{0,0}(x),$$

which possesses a discontinuity on the plane surface $\Sigma_0=\{x=0\}$. We next consider a small perturbation $\mathbf{U}^\delta$ of the solution $\mathbf{U}_0$,

$$\mathbf{U}^\delta(t=0,x,\mathbf{y})=\mathbf{U}_{0,0}(x)+\delta\mathbf{U}_{1,0}(x,\mathbf{y}).$$

$\mathbf{U}^\delta$ satisfies Eq. (A1) and we assume that $\mathbf{U}^\delta$ possesses a discontinuity along the interface Σ^δ,

$$\Sigma^\delta=\{(t,x,\mathbf{y}),x=\eta^\delta(t,\mathbf{y}),t\geqslant 0,\mathbf{y}\in\mathbb{R}^d\}$$

with $\eta^\delta(t=0,\mathbf{y})=\delta\eta_{1,0}(\mathbf{y})$. We consider the frame moving with the interface

$$\tilde{x}=x-\eta^\delta(t,\mathbf{y}),$$

$$\tilde{\mathbf{U}}^\delta(t,\tilde{x},\mathbf{y})=\mathbf{U}^\delta[t,\tilde{x}+\eta^\delta(t,\mathbf{y}),\mathbf{y}].$$

In this frame $\tilde{\mathbf{U}}^\delta$ is discontinuous along the constant interface $\tilde{x}=0$ so we can expand $\tilde{\mathbf{U}}^\delta$ and η^δ as

$$\tilde{\mathbf{U}}^\delta(t,\tilde{x},\mathbf{y})=\tilde{\mathbf{U}}_0(t,\tilde{x})+\delta\tilde{\mathbf{U}}_1(t,\tilde{x},\mathbf{y})+\delta^2\tilde{\mathbf{U}}_2(t,\tilde{x},\mathbf{y})+O(\delta^3),$$

$$\eta^\delta(t,\mathbf{y})=\delta\eta_1(t,\mathbf{y})+\delta^2\eta_2(t,\mathbf{y})+O(\delta^3).$$

Obviously we have $\tilde{\mathbf{U}}_0(t,\tilde{x})=\mathbf{U}_0(t,\tilde{x})$ and $\tilde{\mathbf{U}}_j, j=0, 1, 2$, is the sum of a smooth function and a distribution whose support is the surface $\tilde{x}=0$. Let us introduce a notation. Given a function $\tilde{x}\mapsto\tilde{\phi}(\tilde{x})$ which is smooth except at the point $\tilde{x}=0$ where it presents a jump discontinuity, we define $\{\partial_{\tilde{x}}\tilde{\phi}\}$ by $\partial_{\tilde{x}}\tilde{\phi}=\{\partial_{\tilde{x}}\tilde{\phi}\}+[\tilde{\phi}_0]\delta_0$, where $[\tilde{\phi}_0]=\tilde{\phi}(0^+)-\tilde{\phi}(0^-)$. In other words, $\{\partial_{\tilde{x}}\tilde{\phi}\}$ is the "function part" of the distribution derivative $\partial_{\tilde{x}}\tilde{\phi}$ of $\tilde{\phi}$. It appears that it is convenient to work with the variables $\overline{\mathbf{U}_j}$ defined by

$$\overline{\mathbf{U}_1}(t,\tilde{x},\mathbf{y})=\tilde{\mathbf{U}}_1(t,\tilde{x},\mathbf{y})-\eta_1\{\partial_{\tilde{x}}\tilde{\mathbf{U}}_0\}(t,\tilde{x}),$$

$$\overline{\mathbf{U}_2}(t,\tilde{x},\mathbf{y})=\tilde{\mathbf{U}}_2(t,\tilde{x},\mathbf{y})-\eta_2\{\partial_{\tilde{x}}\tilde{\mathbf{U}}_0\}(t,\tilde{x})-\eta_1\{\partial_{\tilde{x}}\tilde{\mathbf{U}}_1\}(t,\tilde{x},\mathbf{y})+\tfrac{1}{2}\eta_1^2\{\partial_{\tilde{x}}^2\tilde{\mathbf{U}}_0\}(t,\tilde{x}).$$

Linear perturbation. $(\overline{\mathbf{U}_1},\eta_1)$ satisfies the linear system $(t\geqslant 0,\mathbf{y}\in\mathbb{R}^d,\tilde{x}\neq 0)$

$$\partial_t[\mathbf{Dh}(\mathbf{U}_0)\overline{\mathbf{U}_1}]+\partial_{\tilde{x}}[\mathbf{Df}(\mathbf{U}_0)\overline{\mathbf{U}_1}]+\sum_{j=1}^{d}\partial_{y_j}[\mathbf{Dg}_j(\mathbf{U}_0)\overline{\mathbf{U}_1}]-\mathbf{Ds}(\mathbf{U}_0)\overline{\mathbf{U}_1}=0, \tag{A2}$$

with the nonzero initial conditions $\overline{\mathbf{U}_1}(t=0,\tilde{x},\mathbf{y})=\mathbf{U}_{1,0}(\tilde{x},\mathbf{y})$ and the Rankine Hugoniot jump conditions at $\tilde{x}=0$,

$$[\mathbf{Df}(\mathbf{U}_0)\overline{\mathbf{U}_1}+\eta_1\mathbf{s}(\mathbf{U}_0)]_0=\left[\partial_t[\eta_1\mathbf{h}(\mathbf{U}_0)]+\sum_{j=1}^{d}\partial_{y_j}[\eta_1\mathbf{g}_j(\mathbf{U}_0)]\right]_0. \tag{A3}$$

Second-order weakly nonlinear perturbation. $(\overline{\mathbf{U}_2},\eta_2)$ satisfies the linear system $(t\geqslant 0,\mathbf{y}\in\mathbb{R}^d,\tilde{x}\neq 0)$

$$\partial_t[\mathbf{Dh}(\mathbf{U}_0)\overline{\mathbf{U}}_2] + \partial_{\tilde{x}}[\mathbf{Df}(\mathbf{U}_0)\overline{\mathbf{U}}_2] + \sum_{j=1}^{d} \partial_{y_j}[\mathbf{Dg}_j(\mathbf{U}_0)\overline{\mathbf{U}}_2] - \mathbf{Ds}(\mathbf{U}_0)\overline{\mathbf{U}}_2 = -\frac{1}{2}\partial_t[\mathbf{D}^2\mathbf{h}(\mathbf{U}_0)(\overline{\mathbf{U}}_1,\overline{\mathbf{U}}_1)] - \frac{1}{2}\partial_{\tilde{x}}[\mathbf{D}^2\mathbf{f}(\mathbf{U}_0)(\overline{\mathbf{U}}_1,\overline{\mathbf{U}}_1)] - \frac{1}{2}\sum_{j=1}^{d} \partial_{y_j}[\mathbf{D}^2\mathbf{g}_j(\mathbf{U}_0)(\overline{\mathbf{U}}_1,\overline{\mathbf{U}}_1)] + \frac{1}{2}\mathbf{D}^2\mathbf{s}(\mathbf{U}_0)(\overline{\mathbf{U}}_1,\overline{\mathbf{U}}_1), \tag{A4}$$

with zero-initial conditions $\overline{\mathbf{U}}_2(t=0,\tilde{x},\mathbf{y})=\mathbf{0}$, source terms quadratic in $\overline{\mathbf{U}}^1$, and the jump conditions at $\tilde{x}=0$:

$$\left[\mathbf{Df}(\mathbf{U}_0)\overline{\mathbf{U}}_2 + \tfrac{1}{2}\mathbf{D}^2\mathbf{f}(\mathbf{U}_0)(\overline{\mathbf{U}}_1,\overline{\mathbf{U}}_1)\,\eta_2\mathbf{s}(\mathbf{U}_0) + \eta_1\mathbf{Ds}(\mathbf{U}_0)\overline{\mathbf{U}}_1 + \tfrac{1}{2}\eta_1^2\mathbf{Ds}(\mathbf{U}_0)\partial_{\tilde{x}}\mathbf{U}_0\right]_0 = \left[\partial_t\left(\eta_2\mathbf{h}(\mathbf{U}_0) + \eta_1\mathbf{Dh}(\mathbf{U}_0)\overline{\mathbf{U}}_1 + \tfrac{1}{2}\eta_1^2\mathbf{Dh}(\mathbf{U}_0)\partial_{\tilde{x}}\mathbf{U}_0\right) + \sum_{j=1}^{d}\partial_{y_j}\left(\eta_2\mathbf{g}_j(\mathbf{U}_0) + \eta_1\mathbf{Dg}_j(\mathbf{U}_0)\overline{\mathbf{U}}_1 + \tfrac{1}{2}\eta_1^2\mathbf{Dg}_j(\mathbf{U}_0)\partial_{\tilde{x}}\mathbf{U}_0\right)\right]_0. \tag{A5}$$

The system (1)–(3) can be cast into the form (A1) by taking $d=2, \mathbf{U}=(\rho,u,v_1,v_2,p)$,

$$\mathbf{h}(\mathbf{U}) = \begin{pmatrix} \rho \\ u \\ v_1 \\ v_2 \end{pmatrix}, \quad \mathbf{f}(\mathbf{U}) = \begin{pmatrix} \rho u \\ \rho u^2 + p \\ \rho u v_1 \\ \rho u v_2 \end{pmatrix}, \quad \mathbf{s}(\mathbf{U}) = \begin{pmatrix} 0 \\ \rho g \\ 0 \\ 0 \end{pmatrix},$$

$$\mathbf{g}_1(\mathbf{U}) = \begin{pmatrix} \rho v_1 \\ \rho u v_1 \\ \rho v_1^2 + p \\ \rho v_1 v_2 \end{pmatrix}, \quad \mathbf{g}_2(\mathbf{U}) = \begin{pmatrix} \rho v_2 \\ \rho u v_2 \\ \rho v_1 v_2 \\ \rho v_2^2 + p \end{pmatrix}.$$

In the SBM model the density is uniform in each domain $\rho_0(x>0)=\rho_R, \rho_0(x<0)=\rho_L$, and the density perturbations are neglected $\overline{\rho_1}=\overline{\rho_2}=0$. Finally the system is complemented with the energy conservation relation (4). This equation is treated separately because the SBM approximation is applied only to the hydrodynamic variables and not to the temperature. As a result, the temperature and the heat flow are continuous.

[1] J. D. Lindl, *Inertial Confinement Fusion* (Springer, New York, 1998).
[2] S. E. Bodner, Phys. Rev. Lett. **33**, 761 (1974).
[3] J. Sanz, Phys. Rev. Lett. **73**, 2700 (1994).
[4] V. N. Goncharov, R. L. Betti, R. L. McCrory, P. Sorotokin, and C. P. Verdon, Phys. Plasmas **3**, 1402 (1996).
[5] J. W. Jacobs and I. Catton, J. Fluid Mech. **187**, 329 (1988).
[6] J. Sanz, J. Ramirez, R. Ramis, R. Betti, and R. P. J. Town, Phys. Rev. Lett. **89**, 195002 (2002).
[7] T. Ikegawa and K. Nishihara, Phys. Rev. Lett. **89**, 115001 (2002).
[8] H. J. Kull and S. I. Anisimov, Phys. Fluids **29**, 2067 (1986).
[9] A. R. Piriz, J. Sanz, and L. F. Ibanez, Phys. Plasmas **4**, 1117 (1997).
[10] A. R. Piriz, Phys. Plasmas **8**, 997 (2001).
[11] L. Masse, Ph.D. thesis, Université de Provence, 2001.
[12] P. Clavin and L. Masse, Phys. Plasmas **11**, 690 (2004).
[13] R. Adler, *The Geometry of Random Fields* (Wiley, New York, 1981).
[14] H. J. Kull, Phys. Rep. **206**, 197 (1991).
[15] S. W. Haan, Phys. Fluids B **3**, 2349 (1991).
[16] J. Garnier, P. -A. Raviart, C. Cherfils-Clérouin, and L. Masse, Phys. Rev. Lett. **90**, 185003 (2003).
[17] M. Berning and A. M. Rubenchik, Phys. Fluids **10**, 1564 (1998).
[18] S. W. Haan, Phys. Rev. A **39**, 5812 (1989).
[19] R. Betti, V. N. Goncharov, R. L. McCrory, and C. P. Verdon, Phys. Plasmas **5**, 1446 (1998).
[20] J. Sanz, Phys. Rev. E **53**, 4026 (1996).
[21] H. J. Kull, Phys. Fluids B **1**, 170 (1989).
[22] D. Ofer, U. Alon, D. Shvarts, R. L. McCrory, and C. P. Verdon, Phys. Plasmas **3**, 3073 (1996).
[23] J. P. Dahlburg, D. E. Fyve, G. H. Gardner, S. W. Haan, S. E. Bodner, and G. D. Doolen, Phys. Plasmas **2**, 2453 (1995).
[24] M. J. Dunning and S. W. Haan, Phys. Plasmas **2**, 1669 (1995).
[25] B. A. Remington, S. V. Weber, M. M. Marinak, S. W. Haan, J. D. Kilkenny, R. J. Wallace, and G. Dimonte, Phys. Plasmas **2**, 241 (1995).
[26] E. Buresi, J. Coutant, R. Dautray, M. Decroisette, B. Duborgel, P. Guillaneux, J. Launspach, P. Nelson, C. Patou, J.-M. Reisee *et al.*, Laser Part. Beams **4**, 531 (1986).
[27] V. N. Goncharov, P. McKenty, S. Skupsky, R. Betti, R. L. McCrory, and C. Cherfils-Clérouin, Phys. Plasmas **7**, 5118 (2000).
[28] V. N. Goncharov, Phys. Rev. Lett. **82**, 2091 (1999).
[29] P. -A. Raviart and E. Godlewski, Laboratoire d'Analyse Numérique, Paris Technical Report No. R03, 2000 (unpublished).